Verification of quantum-gate teleportation based on Bell nonlocality in a black-box scenario

Zi-Qi Wang and Tie-Jun Wang ⬤*

State Key Laboratory of Information Photonics and Optical Communications and School of Science,
Beijing University of Posts and Telecommunications, Beijing 100876, China

Quantum gate teleportation (QGT) is an excellent candidate for implementing remote quantum gate operations in large-scale quantum computer networks as it has the minimum resource demand to realize such computing models. The Bell nonlocality of quantum entanglement channel in QGT can be transformed into the corresponding posterior statistics correlation obtained by local measurements after QGT operation, and this Bell-type-like correlation can be used to check device and measurement loopholes or information leaking in the teleportation systems. In this paper, we propose a verification scheme based on Bell nonlocality for quantum CNOT gate teleportation in a black-box scenario where the vendors may not be trusted. The double criteria of high fidelity ($\bar{F} > 97.53\%$) and high CHSH inequality violation (CHSH > 2) are used for assessing a vendor's reliability. The clients can use our scheme to check whether vendors employ classical simulation techniques to forge nonlocal quantum computing processes and it could provide a secure manner for the construction of quantum computer networks in the future.

I. INTRODUCTION

Quantum teleportation (QT) [1] plays an important role in the field of quantum information. It allows two remote parties, the sender Alice and the receiver Bob, to use a shared quantum maximally entangled state to transfer an unknown quantum state without exchanging the physical system itself. Quantum gate teleportation (QGT) [2] is an important extension of QT, and QGT realizes the direct teleportation of quantum controlled gates. In quantum networks, QGT is considered to be a basic component of distributed quantum computing [3,4], and it has the minimum communication cost (one shared quantum entanglement pair and two classical bits) [5–7] for the realization of remote-controlled quantum computing models, which is of great significance for the the construction of large-scale quantum computers in the future [2,8,9]. Both the theoretical schemes [7,10–13] and the experimental implementation of QGT [5,6,14] have been achieved.

Optimal QT or QGT works under the assumption that all parties are trusted and the state of quantum channel is maximally entangled. However, there may be physical imperfections in the devices and measurement. Especially because of the precious of quantum maximally entangled state resources, the untrusted vendors may use classical simulation techniques to replace quantum resources. Factors like these can lead to not only a lower teleportation fidelity but also the information leaking in teleportation. Fortunately, relevant research has found that, regardless of the functioning of the devices and quantum channels involved, the security and reliability of QT implementation can be deduced from the observed local measurement outcomes of the QT [15,16].

In 1994, Popescu proved that if the two communicating parties share no entanglement, the average fidelity for the teleportation of an unknown quantum state is limited by $\bar{F} = \frac{2}{3}$ [17]. In 1996, Gisin's work made this criterion no longer credible and it proved that a average fidelity of 0.87 can be achieved when only classic resources were used for simulating a quantum-state teleportation [18] (exceeding the bound of $\bar{F} = \frac{2}{3}$). Besides the fidelity, the Bell nonlocality correlation is introduced in a quantum teleportation verification and the device-independent (DI) manner, which is initially introduced in quantum key distribution [19–22], can also be used to check quantum state teleportation processing. Through the study of the relationship between Bell's theorem [23] and quantum teleportation, the work of Clifton and Pope [15] showed that the condition of average fidelity $\bar{F} > 0.9$ would guarantee that the observed teleportation result is not simulated by local variables. However, in the situation of using active compensation information for calculation, the possibility for vendors to steal and fake information has been proven [24]. In 2013, Ho *et al.* proposed a new protocol to classically simulate a one-way quantum-state teleportation with an average fidelity of 0.97 [16]. Ho also proposed a new device-independent verification scheme for QT, which can verify the absence of such high-fidelity classical simulations by using only posterior statistics [16]. However, these DI verification schemes of QT cannot be directly applied to the QGT process because the process of QGT is more complex than QT.

As QGT is a two-way quantum information transmission process, the target system of QGT has changed from a qubit in QT to a quantum gate composed of two-qubits of the two communication parties, which also leads to that the dimensions of the whole target system is raised from three-dimensional to 15-dimensional in the quantum Bloch-vector space description [25]. When designing a nonlocality verification scheme of

----
*wangtiejun@bupt.edu.cn

QGT, Bell nonlocality in quantum entanglement channel will be projected into a 15-dimensional space, and the corresponding local measurements required for posterior statistics may become more complex than the ones in QT. If only performing local measurements as in previous DI-QT schemes [16], the CHSH inequality will not be violated with probability distributions achieved in QGT scheme.

In this paper, we construct a CHSH-type verification scheme for quantum CNOT gate teleportation. In this scheme, we give the form of the probability distributions of four-qubit measurements results in the QGT scheme, bring it into the CHSH inequality [26] to find the region where the inequality violates, and prove that Bell nonlocality of the black-box system can be measured with our manner. With the CHSH value > 2 criteria alone, one can only verify whether the vendor use enough entanglement resources to perform a CNOT teleportation; but combined with the criteria of average fidelity $\bar{F} > 97.53\%$, one can also check whether vendors employ classical simulation techniques to eavesdrop information and forge nonlocal quantum computing processes. As any natural building blocks for quantum algorithms can be achieved by combining CNOT gates and single-qubit rotations [27], this scheme not only is a verification of the security and reliability of of QGT, but also provides a secure manner for the construction of quantum computer networks in the future.

This paper is organized as follows. In Sec. II, we first review the QGT system of a CNOT gate and introduce a description of the present proposal in the black-box scenario (Sec. II A); and then we give the geometry description for a two-qubits system using generalized Bloch vectors in the 15-dimensional real vector space (Sec. II B); finally, we give the measurements for Bell nonlocality verification process design in the case of black-boxes and give the form of the probability distributions of four-qubit measurements results in the QGT scheme (Sec. II C). Based on this, in Sec. III, we brought the probability distributions of measurements results into the CHSH inequality, gave the form of corresponding CHSH values, and discuss the relationship between observed inequality violations and system performance. In Sec. IV, we discussed the high fidelity classical simulation scheme of the quantum CNOT gate teleportation system, and analyzed the security assessment of the black-box system in the presence of eavesdropping and classical simulation. Finally, we give the conclusion and summary in Sec. V.

II. QGT VERIFICATION PROPOSAL IN BLACK-BOX SCENARIO

In this section, we review the construction of a nonlocal quantum CNOT gate [5–7,10–12], introduce the Bell nonlocality verification proposal of the nonlocal quantum CNOT gate teleportation (CNOT-QGT) in the black-box scenario, and give the geometry description of the present proposal [25,28] and the probability distributions of measurements results in verification proposal.

A. Quantum teleportation of a CNOT gate

Assume that there are two independent users Alice and Bob who each hold one qubit A or B, and they need to perform a nonlocal quantum CNOT gate on qubits A and B (as
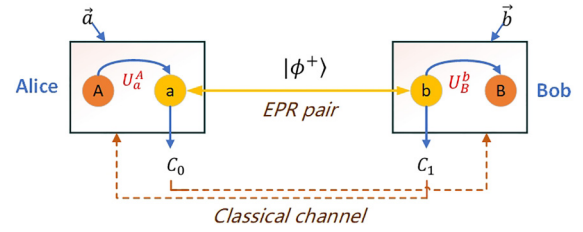

FIG. 1. The description of the quantum CNOT gate teleportation. In this system scheme, Alice and Bob share a pair of EPR pairs, U_a^A and U_B^b represent local quantum CNOT gates. For U_a^A, A is the control qubit and a is the target qubit. Similarly, for U_B^b, b is the control bit and B is the target qubit. Alice's and Bob's boxes have additional classical information input. These information c_0 and c_1 represent the single-qubit measurement results of qubits a and b in the corresponding measurement basis, respectively. Wherein, c_0 is the measurement result of Alice's entangled qubit a, which is sent to Bob through the classical communication channel, and c_1 is the measurement result of Bob's entangled qubit b, which is sent to Alice through the classical communication channel.

shown in Fig. 1).[1] Meanwhile, Alice and Bob share a pair of maximally entangled qubits (a, b) through the black-box devices provided by the vendor, and the state of entangled qubits is $|\phi^+\rangle = \frac{1}{\sqrt{2}}(|00\rangle + |11\rangle)_{ab}$. In Alice's black box, there is a local CNOT gate operation performed on the qubit A which state is $|\psi\rangle_A = \alpha|0\rangle + \beta|1\rangle$ and the entangled qubit a, and here, A is the control qubit. Then, Alice performs a measurement on qubit a in the measurement basis $M_Z \in \{|0\rangle, |1\rangle\}$, and sends the outputs $c_0 \in \{0, 1\}$ to Bob through the classic channel. Similarly, in Bob's box, there is also a CNOT gate operation between the entangled qubit b and the input qubit B ($|\psi\rangle_B = \gamma|0\rangle + \xi|1\rangle$), where b is the control qubit. Bob measures qubit b in the measurement basis $M_X \in \{|0\rangle_X = \frac{1}{\sqrt{2}}(|0\rangle + |1\rangle), |1\rangle_X = \frac{1}{\sqrt{2}}(|0\rangle - |1\rangle)\}$ and sends the measurement outcome $c_1 \in \{0, 1\}$ to Alice. Then, according to the result of active compensation information ($c_0 c_1 \in \{00, 01, 10, 11\}$), Alice and Bob further perform the corresponding unitary operations ($\{\mathbb{I}_A \otimes \mathbb{I}_B, \sigma_A^z \otimes \mathbb{I}_B, \mathbb{I}_A \otimes \sigma_B^x, -\sigma_A^z \otimes \sigma_B^x\}$) on the qubits A and B, respectively, and complete the teleportation of a nonlocal CNOT gate. Where $\sigma_A^z = \left(\begin{smallmatrix} 1 & 0 \\ 0 & -1 \end{smallmatrix}\right)_A$ and $\sigma_B^x = \left(\begin{smallmatrix} 0 & 1 \\ 1 & 0 \end{smallmatrix}\right)_B$ are the corresponding Pauli operator operations on the corresponding qubit.

The vendor of quantum computing can integrate the above processes into two boxes connected by classical channels and quantum channels. After Alice and Bob purchase the boxes that allegedly can perform quantum gate teleportation and the related nonlocal computing function, they, respectively, input one-qubit that they want to realize remote quantum gate operation into the boxes. If the vendor of QGT is untrustworthy, he claims that Alice and Bob are conducting with quantum resources. However, he actually only gave a high-fidelity simulation using classical communications. Due to the lack of prior evidence, it is impossible to judge whether

---

[1] The simulation of pure state situations is the most demanding for teleportation. Therefore, in this study, we only focus on pure-state input situations [16].
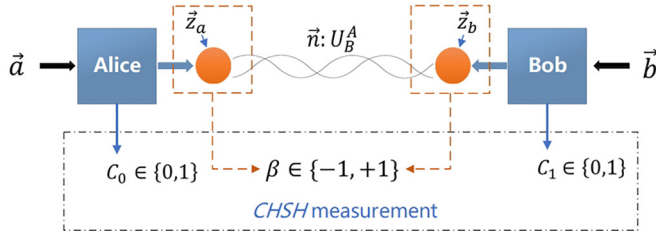
FIG. 2. A verification scheme for the black-box of the two-qubits QGT. In this scheme, there is no active compensation information between the two black-boxes. $\vec{a}$ and $\vec{b}$ represents Alice's and Bob's black-box input states, respectively. The inputs of Alice and Bob are independent. After transmission by the QGT system, the output target state $\vec{n}$ is the remote controlled CNOT gate state U_B^A between Alice and Bob. c_0 and c_1 are the black-box output results of Alice and Bob, respectively. After QGT transmission, local measurement $\vec{z}_a$ and $\vec{z}_b$ are performed on the output states of Alice and Bob, respectively, and independently, and the corresponding joint measurement results β can be obtained.

the vendor's statement is credible for Alice and Bob, especially when active compensation [24] is included, as shown in Fig. 1. Active compensation is the process of publishing the additional two bit input information (c_0, c_1) of Alice's and Bob's boxes, which also provides more leeway for the vendor to fake [16,24]. In fact, relevant research has proven that with the active compensation, perfect teleportation can be faked by purely classical methods [16,24,29]. Therefore, one needs to verify the quantum nature of the black-box system by observing the posterior statistical outcomes. In addition for this untrusted vendor issue, we will take the CNOT-QGT black-box system as an example to discuss the posteriori quantum resource verification scheme of QGT. As shown in Fig. 2, in a nonlocal verification scheme, the QGT implementation system should be built first, and completing the basic QGT process without publishing two bits of classical information (c_0, c_1) (measurements results by performing detection on entangled channel-qubits). Then, Alice's and Bob's qubits A and B are measured and they publish all results by classical communication to obtain statistical results through repeated experiments. One can bring statistical results into the CHSH inequality and prove that Bell nonlocality can be measured using this method.

B. Bloch-vector description of a four-dimensional system

In quantum mechanics, the Bloch vector space [30–36] can provide an intuitive geometric description of quantum states or quantum operations. For two-dimensional quantum systems, the density matrix representation of quantum state can be expressed as $\rho = |\psi\rangle\langle\psi| = \frac{1}{2}(\mathbb{I}_2 + \vec{n} \cdot \vec{\sigma})$, where, $\vec{\sigma} = (\sigma_1, \sigma_2, \sigma_3)$ is the Pauli operator, and $\vec{n}$ is the Bloch vector corresponding to the quantum state ρ, for the pure state, $|\vec{n}| = 1$ (mixed state $|\vec{n}| < 1$) [30]. Then the Bloch vector corresponding to a two-dimensional quantum pure state $|\psi\rangle$ can be expressed as $\vec{n} = (\sin\theta\cos\phi, \sin\theta\sin\phi, \cos\theta)$, where $\theta \in [0, \pi]$, $\phi \in [0, 2\pi]$, represents the two angle real parameters of the unit Bloch sphere in the $\mathbb{R}^3$, θ represents the zenith angle and ϕ is the azimuth angle [30–33]. The Bloch sphere also can be extended to an N-dimensional quantum system.

For an N-dimensional quantum system, the $N \times N$ density matrix ρ can be represented by a Bloch vector as

$$\rho = \frac{1}{N}\mathbb{I}_N + \frac{1}{2}\sum_{i=1}^{N^2-1} n_i \cdot \lambda_i, \tag{1}$$

where $\mathbb{I}_N$ is $N \times N$ identity matrix and λ_i is the generators of the algebra SU(N) group $\vec{\lambda}$ [28]. In particular, for the SU(2) group, $\vec{\lambda} = \vec{\sigma}$ is the Pauli operator. The $(N^2 - 1)$-dimensional vector $\vec{n} = (n_1, n_2, \ldots, n_{N^2-1})$ is the corresponding generalized Bloch vector for the N-dimensional quantum system [28]. The Bloch vector space is contained in the $(N^2 - 1)$-dimensional space, i.e., $\{\vec{n} \in \mathbb{R}^{N^2-1} : |\vec{n}| \leqslant \sqrt{\frac{2(N-1)}{N}}\}$. Different to the qubit case, however, it was proved [28,37] that when $N \geqslant 3$, the map induced is not bijective: not every point on the "Bloch sphere" in dimensions $N^2 - 1$ corresponds to a physical state [37]. The Bloch vector space is only a part of the hypersphere with radius $\sqrt{\frac{2(N-1)}{N}}$ and the $(N^2 - 1)$-dimensional Bloch vector space has an asymmetric structure ($N \geqslant 3$) [25,28]. In fact, at present, the structure of the Bloch vector space is fully known only when $N = 2$, i.e., the three-dimensional Bloch sphere [25].

For a four-dimensional quantum system m that is composed of two-qubits A, B, the generator of the SU(4) group $\lambda_i (i = 1, 2, \ldots, 15) \in \mathbb{R}^{15}$ is shown in Appendix A. The corresponding Bloch vector space is part of a sphere with radius $\sqrt{\frac{3}{2}}$ in the 15-dimensional vector space. If the two-qubit system is four-dimensional completely separable that can be represented as a tensor product of two two-dimensional systems, i.e., $\rho_m = \rho_A \otimes \rho_B$. In addition, the ρ_A ($|\psi\rangle_A$) and ρ_B ($|\psi\rangle_B$) can be expressed as a three-dimensional Bloch vector $\vec{a} = (a_1, a_2, a_3) = (\sin\theta\cos\phi, \sin\theta\sin\phi, \cos\theta)$ and $\vec{b} = (b_1, b_2, b_3) = (\sin\eta\cos\upsilon, \sin\eta\sin\upsilon, \cos\eta)$ respectively, where θ and ϕ are the angle real parameters of Bloch ball corresponding to Alice. Similarly, η and υ are the angle parameters corresponding to Bob. Also, $\theta, \eta \in [0, \pi]$ represents the zenith angle, $\phi, \upsilon \in [0, 2\pi]$ are the azimuth angles [30,31,36]. According to Eq. (1), one can denote the separable product state ρ_m into a 15-dimensional Bloch vector $\vec{m} = (m_1, m_2, \ldots, m_{15})$, and the components $m_i (i = 1, 2, \ldots, 15)$ of the vector $\vec{m}$ can be computed in terms of components of the Bloch vectors $\vec{a}$ and $\vec{b}$ using explicit realization of the generators of SU(4) [25]

$$m_1 = \frac{b_1}{2}(1 + a_3), \ m_2 = \frac{b_2}{2}(1 + a_3), \ m_3 = \frac{b_3}{2}(1 + a_3),$$

$$m_4 = \frac{a_1}{2}(1 + b_3), \ m_5 = \frac{a_2}{2}(1 + b_3),$$

$$m_6 = \frac{1}{2}(a_1 b_1 + a_2 b_2), \ m_7 = \frac{1}{2}(a_2 b_1 - a_1 b_2),$$

$$m_8 = \frac{1}{2\sqrt{3}}(a_3 b_3 + 2a_3 - b_3),$$

$$m_9 = \frac{1}{2}(a_1 b_1 - a_2 b_2), \ m_{10} = \frac{1}{2}(a_1 b_2 + a_2 b_1),$$

$$m_{11} = \frac{a_1}{2}(1 - b_3), \ m_{12} = \frac{a_2}{2}(1 - b_3),$$

$$m_{13} = \frac{b_1}{2}(1 - a_3), \ m_{14} = \frac{b_2}{2}(1 - a_3),$$

$$m_{15} = \frac{1}{\sqrt{6}}(a_3 + b_3 - a_3 b_3). \tag{2}$$

After a perfect nonlocal CNOT operation on qubits A and B, the corresponding density matrix of the system AB becomes $\rho_{A,B} = \frac{1}{4}\mathbb{I}_4 + \frac{1}{2}(\vec{n} \cdot \vec{\lambda})$. The elements $n_i (i = 1, 2, \ldots, 15)$ of 15-dimensional Bloch vectors $\vec{n}$ of this two-qubit system are shown as follows:

$$n_1 = \frac{b_1}{2}(1 + a_3), \ n_2 = \frac{b_2}{2}(1 + a_3), \ n_3 = \frac{b_3}{2}(1 + a_3),$$

$$n_4 = \frac{1}{2}(a_1 b_1 - a_2 b_2), \ n_5 = \frac{1}{2}(a_1 b_2 + a_2 b_1),$$

$$n_6 = \frac{a_1}{2}(1 - b_3), \ n_7 = \frac{a_2}{2}(1 - b_3),$$

$$n_8 = \frac{1}{2\sqrt{3}}(2a_3 + b_3 - a_3 b_3),$$

$$n_9 = \frac{a_1}{2}(1 + b_3), \ n_{10} = \frac{a_2}{2}(1 + b_3),$$

$$n_{11} = \frac{1}{2}(a_1 b_1 + a_2 b_2), \ n_{12} = \frac{1}{2}(a_2 b_1 - a_1 b_2),$$

$$n_{13} = \frac{b_1}{2}(1 - a_3), \ \ n_{14} = \frac{b_2}{2}(a_3 - 1),$$

$$n_{15} = \frac{1}{\sqrt{6}}(a_3 - b_3 + a_3 b_3). \tag{3}$$

In addition, as the ideal quantum gate teleportation process was described in Sec. II A, with (c_0, c_1) as the condition, the teleportation state is contained in the boxes for

$$\rho_{A,B} = \frac{1}{4}\mathbb{I}_4 + \frac{1}{2}[\vec{n}' \cdot \vec{\lambda}] = \frac{1}{4}\mathbb{I}_4 + \frac{1}{2}[(R_{c_0,c_1} \cdot \vec{n}) \cdot \vec{\lambda}], \tag{4}$$

where $\vec{n}' = R_{c_0,c_1} \cdot \vec{n}$, $R_{00} = \mathbb{I}$, $R_{01} = R_a(\hat{z}, \pi)$, $R_{10} = R_b(\hat{x}, \pi)$, $R_{11} = R_a(\hat{z}, \pi)$ & $R_b(\hat{x}, \pi)$. The 15-dimensional unitary matrix form of R_{c_0,c_1} is shown in Appendix B.

C. Measurement description of quantum CNOT gate teleportation in the black-box scenario

As the internal workings of the black boxes are not visible, a posterior verification approach is necessary for Alice and Bob to avoid being deceived by the vendor. The verification method based on the Bell nonlocality is shown in Fig. 2. Alice and Bob can only compare the posterior results with the expected results. Therefore, in such a black-box scenario, Alice and Bob should be trusted for their respective input states, and share a common reference frame for preparing the inputs and measuring the outputs [16]. At the same time, without active compensation, the observed phenomena are not affected by local factors and meet the space-like separation relationship for the relevant events of the Bell test.

After CNOT-QGT, Alice and Bob each independently perform a measurement on the subsystem A and B along the direction $\vec{z}_a$ and $\vec{z}_b$, respectively, where $\vec{z}_a = (x_a, y_a, z_a)$ and $\vec{z}_b = (x_b, y_b, z_b)$. The 15-dimensional Bloch vector $\vec{z}$ denotes a separable four-dimensional quantum state $\rho_{\vec{z}}$ formed by two one-qubit states $\rho_{\vec{z}_a}$ and $\rho_{\vec{z}_b}$ which are denoted by two three-dimensional Bloch vectors $\vec{z}_a$ and $\vec{z}_b$, respectively, namely, $\rho_{\vec{z}} = \rho_{\vec{z}_a} \otimes \rho_{\vec{z}_b}$. According to the definition

and properties of operator fidelity [38], the measurement results of Alice and Bob are linearly distributed with $\vec{z}_a$ and $\vec{z}_b$, respectively [16]. That is, there are four corresponding measuring projection directions for $\vec{z}$: $|z^1\rangle \rightarrow \rho_{\vec{z}^1} = \rho_{\vec{z}_a} \otimes \rho_{\vec{z}_b}$, $|z^2\rangle \rightarrow \rho_{\vec{z}^2} = \rho_{-\vec{z}_a} \otimes \rho_{-\vec{z}_b}$, $|z^3\rangle \rightarrow \rho_{\vec{z}^3} = \rho_{-\vec{z}_a} \otimes \rho_{\vec{z}_b}$, $|z^4\rangle \rightarrow \rho_{\vec{z}^4} = \rho_{\vec{z}_a} \otimes \rho_{-\vec{z}_b}$. Here, $\rho_{\vec{x}} = \frac{1}{N}\mathbb{I}_N + \frac{1}{2}(\vec{x} \cdot \vec{\lambda})$ and $\rho_{-\vec{x}} = \frac{1}{N}\mathbb{I}_N + \frac{1}{2}(-\vec{x} \cdot \vec{\lambda})$, the relationship between the above qubit state $\rho_{\vec{x}}$ and the corresponding Bloch vector $\vec{x}$ is given by Eq. (1). The form of the 15-dimensional Bloch vector $|z^j\rangle$ ($j = 1, 2, 3$, and 4) is shown in Appendix B. Then, the joint measurement output result is recorded as $\beta = +1$ when Alice and Bob measuring projection directions are $\vec{z}_a$ and $\vec{z}_b$, respectively (correspondingly, the joint measurement result is $\vec{z} = \vec{z^1}$); otherwise, the joint measurement output results are recorded as $\beta = -1$ (correspondingly, the joint measurement result is $\vec{z^2}, \vec{z^3}$, or $\vec{z^4}$). Meanwhile, the output of Alice's classical bit is $c_0 \in \{0, 1\}$, and Bob's classical bit is $c_1 \in \{0, 1\}$. For each group of randomly selected inputs vectors and measurement direction are $\vec{a}, \vec{b}, \vec{z}_a$, and $\vec{z}_b$. One can obtain the corresponding group $\{\vec{n}, \vec{z}\} \in \mathbb{R}^{15}$. Assuming that there is no active compensation in the system and the input states are credible, one can extract the probability distributions $P(c_0, c_1, \beta | \vec{n}, \vec{z})$. In the ideal case, the probability $P(\beta = +1 | c_0, c_1, \vec{n}, \vec{z})$ is

$$P(\beta = +1) = \text{Tr}[\rho_{A,B} \cdot \rho_{\vec{z^1}}] = \frac{1}{4}[1 + 2(R_{c_0,c_1} \cdot \vec{n}) \cdot \vec{z}]. \tag{5}$$

Similarly, the probability $P(\beta = -1 | c_0, c_1, \vec{n}, \vec{z})$ is

$$P(\beta = -1) = \text{Tr}[\rho_{A,B} \cdot \rho_{\vec{z^2}}] + \text{Tr}[\rho_{A,B} \cdot \rho_{\vec{z^3}}] + \text{Tr}[\rho_{A,B} \cdot \rho_{\vec{z^4}}]$$

$$= \frac{1}{4}[3 + 2(R_{c_0,c_1} \cdot \vec{n}) \cdot (\vec{z^2} + \vec{z^3} + \vec{z^4})]$$

$$= \frac{1}{4}[3 - 2(R_{c_0,c_1} \cdot \vec{n}) \cdot \vec{z}]. \tag{6}$$

That is, the probability $P(\beta | c_0, c_1, \vec{n}, \vec{z})$ can be represented as

$$P(\beta = \pm 1 | \vec{z}) = \frac{1}{4}[2 - \beta + 2\beta(R_{c_0,c_1} \cdot \vec{n}) \cdot \vec{z}]. \tag{7}$$

Supposing that Alice and Bob have carried out an infinite number of experiments. From the statistical data of the outcomes, they can obtain the relevant probability distribution $P(c_0, c_1, \beta | \vec{n}, \vec{z})$, which is used to verify the nature of this CNOT-QGT. In an ideal situation, the output of (c_0, c_1) is almost uniformly distributed, and the probability $P(c_0, c_1 | \vec{n}) = \frac{1}{4}$. The measurement result β has a linear distribution with $\vec{z}$; then, the relevant probability distribution is

$$P(c_0, c_1, \beta | \vec{n}, \vec{z}) = \frac{1}{16}[2 - \beta + 2\beta(R_{c_0,c_1} \cdot \vec{n}) \cdot \vec{z}]. \tag{8}$$

In the situation of active compensation, Alice and Bob can extract a vector $\vec{M}_{c_0 c_1}(\vec{n})$ from the boxes, which is equivalent to $\vec{n}$ in the ideal case. By randomly sampling the state $\vec{M}_{c_0 c_1}(\vec{n})$, the average teleportation fidelity of the average system can be estimated as [16]

$$\bar{F} = \int \frac{d\vec{n}}{S} \sum_{c_0, c_1} P(c_0 c_1) \frac{1 + 2\vec{M}_{c_0,c_1}(\vec{n}) \cdot \vec{n}}{4}. \tag{9}$$

With Eqs. (8) and (9), one can formally carry out the quantum verification of the nonlocal CNOT gate teleportation system.

III. NONLOCALITY VERIFICATION OF QUANTUM CNOT GATE TELEPORTATION

In this section, we will move to the construction of the non-locality verification scheme, based on the black-box scenario. Since the Bell nonlocality test only depends on the statistical correlation between the observed results in the experiment, it is considered to have the minimum equipment assumption requirement [22]. Here, in our verification scheme for CNOT-QGT, the CHSH-type inequality is used to quantify Bell nonlocality.

In the black-box scenario, Alice and Bob can choose from two groups of input states, and correspondingly, they may obtain two 15-dimensional Bloch vectors $\vec{n}_0$ and $\vec{n}_1$ as outputs of the boxes; similarly, they can choose to make a joint measurement in two bases $\vec{z}_0$ and $\vec{z}_1$. The possible input groups of the corresponding two black-boxes are as follows:

$$\rho_{\vec{n}_0} : U_B^A[\rho_{\vec{a}_0} \otimes \rho_{\vec{b}_0}]; \quad \rho_{\vec{n}_1} : U_B^A[\rho_{\vec{a}_1} \otimes \rho_{\vec{b}_1}];$$

$$\rho_{\vec{z}_0} : [\rho_{\vec{z}_{a_0}} \otimes \rho_{\vec{z}_{b_0}}]; \quad \rho_{\vec{z}_1} : [\rho_{\vec{z}_{a_1}} \otimes \rho_{\vec{z}_{b_1}}]. \quad (10)$$

Here, U_B^A stands for the operator of CNOT gate. $\rho_{\vec{a}_j} = \frac{1}{2}(\mathbb{I}_2 + \vec{a}_j \cdot \vec{\sigma})$ and $\rho_{\vec{b}_j} = \frac{1}{2}(\mathbb{I}_2 + \vec{b}_j \cdot \vec{\sigma})$ $(j \in \{0, 1\})$ represent the optional input group of Alice and Bob's black-boxes. Were, $\vec{a}_j = (a_{j1}, a_{j2}, a_{j3}) = (\sin\theta_j \cos\phi_j, \sin\theta_j \sin\phi_j, \cos\theta_j)$ and $\vec{b}_j = (b_{j1}, b_{j2}, b_{j3}) = (\sin\eta_j \cos\upsilon_j, \sin\eta_j \sin\upsilon_j, \cos\eta_j)$, where $\theta_j, \eta_j \in [0, \pi]$ and $\phi_j, \upsilon_j \in [0, 2\pi]$. And $\rho_{\vec{n}_j} = \frac{1}{4}\mathbb{I}_4 + \frac{1}{2}(\vec{n}_j \cdot \vec{\lambda})$ is two-qubit quantum target states corresponding to $\vec{n}_j$, and the elements $n_{ji}(i = 1, 2, \ldots, 15)$ of 15-dimensional Bloch vectors $\vec{n}_j$ can be achieved by Eq. (3). Correspondingly, $\rho_{\vec{z}_k} = \frac{1}{4}\mathbb{I}_4 + \frac{1}{2}(\vec{z}_k \cdot \vec{\lambda})$ $(k \in \{0, 1\})$ is a two-qubit quantum state corresponding to $\vec{z}_k$ as introduced in Sec. II C. In addition, $\rho_{\vec{z}_{a_k}} = \frac{1}{2}\mathbb{I}_2 + \frac{1}{2}(\vec{z}_{a_k} \cdot \vec{\sigma})$ and $\rho_{\vec{z}_{b_k}} = \frac{1}{2}\mathbb{I}_2 + \frac{1}{2}(\vec{z}_{b_k} \cdot \vec{\sigma})$, where $\vec{z}_{a_k} = (x_{ak}, y_{ak}, z_{ak})$ and $\vec{z}_{b_k} = (x_{bk}, y_{bk}, z_{bk})$ represent the optional measurement basis of Alice and Bob when Bell nonlocality verification is performed.

The classical outcome of the black-box system consists of two bits (c_0, c_1). We define that when the output state is $\vec{n}_j$ $(j = 0, 1)$, one can extact one bit $\alpha \equiv 2c_j - 1 \in \{-1, +1\}$. Then one can evaluate $\text{CHSH} = E_{00} + E_{01} + E_{10} - E_{11}$ with

$$\begin{aligned} E_{jk} &\equiv P(\alpha = \beta|j, k) - P(\alpha \neq \beta|j, k) \\ &= P(c_j = 0, \beta = -1|j, k) + P(c_j = 1, \beta = +1|j, k) \\ &\quad - P(c_j = 0, \beta = +1|j, k) - P(c_j = 1, \beta = -1|j, k), \end{aligned}$$

$$(11)$$

where $P(c_j, \beta|j, k) \equiv P(c_j, \beta|\vec{n}_j, \vec{z}_k)$, $j, k \in \{0, 1\}$. If $\text{CHSH} > 2$, in a loophole-free assessment, it means that the communication parties must have shared quantum entanglement.

By considering in a noisy channel, it is further assumed that

$$\vec{V}_{c_0 c_1}(\vec{n}) = \mu R_{c_0 c_1} \vec{n}, \ \mu \in [0, 1]. \quad (12)$$

Here, $\vec{V}_{c_0 c_1}(\vec{n})$ represents the vector shared between Alice's and Bob's boxes in the noisy channel. $\mu \in \{0, 1\}$ represents the noise influence in quantum channel, and it refers to the overlap between actual channel state and Bell state. The

impact of the vendor's replacement of channel-entangled resources also can be denoted by μ. Equation (12) means that, even in the case of active compensation, the system will always automatically retrieve to $\mu\vec{n}$ regardless of c_0, c_1. Thus, the probability $P_{\text{obs}}(c_0, c_1, \beta|\vec{n}, \vec{z})$ in a nosiy channel is

$$P_{\text{obs}}(c_0, c_1, \beta|\vec{n}, \vec{z}) = \frac{1}{16}[2 - \beta + 2\beta \cdot \vec{V}_{c_0 c_1}(\vec{n}) \cdot \vec{z}]. \quad (13)$$

From Eq. (11), the CHSH function of the CNOT gate teleportation in black-box case is

$$\begin{aligned} \text{CHSH} &= \frac{1}{4}(\vec{z}_0 + \vec{z}_1)[\vec{V}_{00}(\vec{n}_0) + \vec{V}_{01}(\vec{n}_0) - \vec{V}_{10}(\vec{n}_0) \\ &\quad - \vec{V}_{11}(\vec{n}_0)] + \frac{1}{4}(\vec{z}_0 - \vec{z}_1)[\vec{V}_{00}(\vec{n}_1) \\ &\quad + \vec{V}_{10}(\vec{n}_1) - \vec{V}_{01}(\vec{n}_1) - \vec{V}_{11}(\vec{n}_1)] \\ &= \mu(\vec{z}_0 + \vec{z}_1) \cdot \vec{n}_0' + \mu(\vec{z}_0 - \vec{z}_1) \cdot \vec{n}_1' \\ &= \mu(f_1 + f_2), \quad (14) \end{aligned}$$

where

$$\begin{aligned} \vec{n}_0' &= \left[0, \frac{b_{02}}{2}(1 + a_{03}), \frac{b_{03}}{2}(1 + a_{03}), \right. \\ &\quad 0, 0, 0, 0, \frac{1}{2\sqrt{3}}(b_{03} - a_{03}b_{03}), 0, 0, 0, 0, \\ &\quad \left. 0, \frac{b_{02}}{2}(a_{03} - 1), \frac{1}{\sqrt{6}}(a_{03}b_{03} - b_{03})\right], \\ \vec{n}_1' &= \left[0, 0, 0, \frac{a_{11}b_{11}}{2}, \frac{a_{12}b_{11}}{2}, \frac{a_{11}}{2}, \frac{a_{12}}{2}, \right. \\ &\quad \left. 0, \frac{a_{11}}{2}, \frac{a_{12}}{2}, \frac{a_{11}b_{11}}{2}, \frac{a_{12}b_{11}}{2}, 0, 0, 0\right], \quad (15) \end{aligned}$$

and

$$\begin{aligned} f_1 &= \frac{1}{2}[b_{02}(y_{b0}z_{a0} + y_{b1}z_{a1}) + b_{02}a_{03}(y_{b0} + y_{b1}) \\ &\quad + b_{03}(z_{b0}z_{a0} + z_{b1}z_{a1}) + b_{03}a_{03}(z_{b0} + z_{b1})], \\ f_2 &= \frac{1}{2}[a_{11}(x_{b0}x_{a0} - x_{b1}x_{a1}) + a_{11}b_{11}(x_{a0} - x_{a1}) \\ &\quad + a_{12}(x_{b0}y_{a0} - x_{b1}y_{a1}) + a_{12}b_{11}(y_{a0} - y_{a1})]. \quad (16) \end{aligned}$$

From Eqs. (14) to (16), it can be found that for a set of inputs and corresponding measurement bases from Alice and Bob, the CHSH value is proportional to the overall noise factor μ of the system. When Alice and Bob select input groups $\{\vec{a}_0 = (0, 0, 1), \vec{b}_0 = (0, 0, 1)\}$, and $\{\vec{a}_1 = (\frac{1}{\sqrt{2}}, \frac{1}{\sqrt{2}}, 0), \vec{b}_1 = (1, 0, 0)\}$, by using the corresponding optimal measurement basis $\{\vec{z}_{a_0} = (\frac{\sqrt{6}}{4}, \frac{\sqrt{6}}{4}, \frac{1}{2}), \vec{z}_{b_0} = (\frac{1}{2}, 0, \frac{\sqrt{3}}{2})\}$, $\{\vec{z}_{a_1} = (-\frac{\sqrt{6}}{4}, -\frac{\sqrt{6}}{4}, \frac{1}{2}), \vec{z}_{b_1} = (\frac{1}{2}, 0, \frac{\sqrt{3}}{2})\}$ (which is the measurement basis to maximize the CHSH value), there is $\text{CHSH}_{\text{max}} = \frac{3\sqrt{3}}{2}\mu \approx 2.598$ in the case of $\mu_{\text{max}} = 1$. The point corresponding to the above input groups that maximizes the CHSH value is $\theta_0 = 0, \theta_1 = \frac{\pi}{2}, \eta_0 = 0, \eta_1 = \frac{\pi}{2}, \phi_1 = \frac{\pi}{4}, \upsilon_1 = 0$, and $\phi_0, \upsilon_0 \in [0, 2\pi]$. Therefore, to make sure the quantumness of the system ($\text{CHSH} > 2$), the noise factor μ should satisfy $\mu \geqslant \frac{4}{3\sqrt{3}} \approx 0.7698$.

In addition, from Eq. (9), one can see that the critical value of the average teleportation fidelity of the quantum nonlocal

CNOT gate is

$$\bar{F} = \int \frac{d\vec{n}}{S} \cdot \frac{1 + 2\vec{V}_{c_0,c_1}(\vec{n}) \cdot \vec{n}}{4} = \frac{1 + 2\mu|\vec{n}|^2}{4}$$

$$\geqslant \frac{1}{4}\left(1 + 3 \cdot \frac{4}{3\sqrt{3}}\right) \approx 0.8274. \qquad (17)$$

From Eq. (17), it can be concluded that for a group of trusted inputs, there is a proportional relationship between the noise factor μ and fidelity. If the impact of overall noise can be expressed with μ alone, the observed CHSH value can reflect the performance of the gate teleportation, as the fidelity is proportional to the CHSH value also and the judgments of the quantumness of QGT system is CHSH > 2 or $\bar{F}$ > 0.8274. However, it was proved that in the QT black-box system, the vendor can make the average fidelity of the QT scheme exceed the critical value under the violation boundary of Bell inequality through classical simulation forgery [16,18]. This makes us have to consider whether there will be a high-fidelity classical simulation occurred in the QGT systems. Therefore, in the next section, we will further study the high-fidelity classical simulation methods in four-dimensional quantum systems and improve our conclusions.

IV. HIGH-FIDELITY CLASSICAL SIMULATION AND SECURITY ANALYSIS OF QUANTUM CNOT GATE TELEPORTATION SYSTEM

A. High-fidelity classical simulation without CHSH > 2

The vendor can simulate a CNOT-QGT process by using a bilateral classical simulation protocol of quantum state teleportation. For example, in Gisin's classical simulation protocol [16,18], the Bloch sphere can be evenly divided into four parts $S_{d_0 d_1}$ (d_0 or $d_1 = 0, 1$), and each part has its center vector $\vec{t}_{d_0 d_1}$ which can be defined as $\vec{t}_{00} = \frac{1}{\sqrt{3}}(+1, +1, +1)$, $\vec{t}_{01} = \frac{1}{\sqrt{3}}(+1, -1, -1)$, $\vec{t}_{10} = \frac{1}{\sqrt{3}}(-1, +1, -1)$, $\vec{t}_{11} = \frac{1}{\sqrt{3}}(-1, -1, +1)$. By using Gisin's protocol, any input vector $\vec{a}$ or $\vec{b} \in S_{d_0 d_1}$ can be replaced by the corresponding $\vec{t}_{d_0 d_1}$. Alice and Bob's boxes can contain a series of nonmaximally entangled states for distribution in advance, such as $U_B^A(\vec{t}_{00} \otimes \vec{t}_{00})$, $U_B^A(\vec{t}_{00} \otimes \vec{t}_{01})$, $U_B^A(\vec{t}_{01} \otimes \vec{t}_{00})$, $U_B^A(\vec{t}_{01} \otimes \vec{t}_{01})$, and so on. There are 16 possible combinations, and the corresponding modified states that can be realized by local operation. These states can replace any input of Alice and Bob. We use two $\vec{t}_{00} \otimes \vec{t}_{00}$ states as the inputs to verify the violation of the CHSH inequality we derived in the black-box scenario. According to the CHSH function in Eq. (14), with the outputs of a series of $U_B^A(\vec{t}_{00} \otimes \vec{t}_{00})$ and related $c_0 c_1$, the corresponding $\text{CHSH}_{\text{max}} \approx 1.5396\mu$, $\mu \in [0, 1]$, which always satisfies CHSH $\leqslant$ 2, and the average teleportation fidelity $\bar{F} \approx 0.76$. The other classical simulation inputs give the same conclusion with the corresponding CHSH $\leqslant$ 2.

Ho *et al.* [16] proposed a quantum teleportation classical simulation protocol with maximum fidelity. In this classical simulation model, for any input, the resultant vectors must have their individual components limited to $\frac{1}{\sqrt{2}}$. That is, for the input $\vec{t} = (x, y, z)$, there are six regions on the bloch sphere where the CHSH value of DI-QT scheme [16] is larger than 2, which are (1) $z > \frac{1}{\sqrt{2}}$; (2) $z < -\frac{1}{\sqrt{2}}$; (3) $x > \frac{1}{\sqrt{2}}$; (4)

$x < -\frac{1}{\sqrt{2}}$; (5) $y > \frac{1}{\sqrt{2}}$; (6) $y < -\frac{1}{\sqrt{2}}$. To prevent any possible violation, the classical simulation imposes limits on the input components in the corresponding regions. For example, if the z component of a Bloch vector is greater than $\frac{1}{\sqrt{2}}$, this input vector can be replaced as

$$\vec{a} = \begin{pmatrix} \sin\theta\cos\phi \\ \sin\theta\sin\phi \\ \cos\theta \end{pmatrix} \mapsto \vec{a}_x^B = \begin{pmatrix} \frac{1}{\sqrt{2}}\cos\phi \\ \frac{1}{\sqrt{2}}\sin\phi \\ \frac{1}{\sqrt{2}} \end{pmatrix} \qquad (18)$$

to ensure that there is no inequality violation.

One can adopt Ho's simulation scheme and apply it to bilateral quantum teleportation. Let us suppose that $\vec{a}_{x0}^B = (\frac{1}{\sqrt{2}}\cos\phi, \frac{1}{\sqrt{2}}\sin\phi, \frac{1}{\sqrt{2}})$, $\vec{b}_{x0}^B = (\frac{1}{\sqrt{2}}\cos\upsilon, \frac{1}{\sqrt{2}}\sin\upsilon, \frac{1}{\sqrt{2}})$, $\vec{a}_{x1}^B = (\frac{1}{\sqrt{2}}\cos\phi', \frac{1}{\sqrt{2}}\sin\phi', \frac{1}{\sqrt{2}})$, and $\vec{b}_{x1}^B = (\frac{1}{\sqrt{2}}\cos\upsilon', \frac{1}{\sqrt{2}}\sin\upsilon', \frac{1}{\sqrt{2}})$ are the inputs to verify the violation of the CHSH inequality in Eq. (14), in the black-box scenario, one can obtain $\text{CHSH}_{\text{max}} \approx 1.866\mu < 2$ with an average teleportation fidelity of $\bar{F} \approx 0.9545$. The other classical simulation inputs give the same conclusion with the corresponding CHSH $\leqslant$ 2. Obviously, there is always no inequality violation and the classical simulation results of Ho's model cannot satisfy the our nonlocality verification scheme.

Ho's scheme needs to compress a three-dimensional Bloch vector in six regions [16]. For the CNOT-QGT scheme, we can propose a classical simulation protocol P_{Gate} in which the three-dimensional input Bloch vector is only compressed in two regions, and it can achieve higher fidelity while avoiding CHSH inequality violations. To construct this protocol, one should abandon the hypothesis requirement of Eq. (12), but only that the compensated $\vec{V}_{c_0 c_1}$ form a consistent description, i.e., $\mu = 1$ and $\forall \vec{n}_x, \exists \vec{n}_x^B$ s.t. $R_{c_0 c_1}\vec{V}_{c_0 c_1}(\vec{n}_x) = \vec{n}_x^B$.

Then, by reviewing the CHSH inequality we previously derived, for each group of inputs $\vec{a}$ and $\vec{b}$, there are two kinds of optimal simulation schemes. For vectors $\vec{a}$ and $\vec{b}$ that do not cause CHSH inequality violations regardless of the measurement basis $\vec{z}$, we have

$$\vec{a} \mapsto \vec{a}_x^B = \vec{a}, \ \vec{b} \mapsto \vec{b}_x^B = \vec{b}, \ \vec{n} \mapsto \vec{n}_x^B = \vec{n}, \qquad (19)$$

which retains its own state.

For the CHSH inequality defined in Eq. (14), according to the maximum CHSH value situation (i.e., using the optimal measurement basis that maximizes the CHSH value), the input range of Alice and Bob that can make CHSH > 2 (inequality violation) is (as shown in Figs. 3 and 4)

(i) $0 \leqslant \theta < 0.4\pi$, $\phi \in [0, 2\pi]$,

$\quad 0 < \eta < 0.32\pi$, $\upsilon \in [0, 2\pi]$,

(ii) $0.276\pi < \theta < 0.724\pi$, $0 \leqslant \phi < 0.57\pi$ *or*

$\quad 1.93\pi < \phi \leqslant 2\pi$

$\quad 0.1\pi < \eta < 0.9\pi$, $0 \leqslant \upsilon < 0.4\pi$ *or*

$\quad 1.6\pi < \upsilon \leqslant 2\pi$. $\qquad (20)$

According to this simulation protocol, to avoid the situation of CHSH > 2, vectors $\vec{a}$ and $\vec{b}$ in this region should be replaced by the assignment vectors $\vec{a}_x^B$ and $\vec{b}_x^B$. Then, to
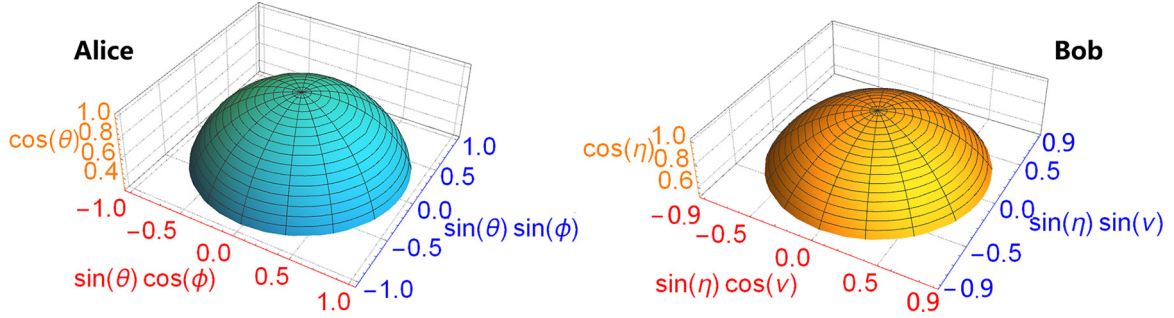
FIG. 3. The first input range of Alice and Bob that makes the inequality violated. The blue arc surface represents Alice's input range and the yellow one represents Bob's input range: $0 \leqslant \theta < 0.4\pi$ and $\phi \in [0, 2\pi]$; $0 < \eta < 0.32\pi$ and $\upsilon \in [0, 2\pi]$.

maximize the simulation average fidelity, our protocol sets the assignment vector as

$$
\vec{a} = \begin{pmatrix} \sin\theta\cos\phi \\ \sin\theta\sin\phi \\ \cos\theta \end{pmatrix} \mapsto \vec{a}_x^B = \begin{pmatrix} \sin(0.37\pi)\cos\phi \\ \sin(0.37\pi)\sin\phi \\ \cos(0.37\pi) \end{pmatrix},
$$

$$
\vec{b} = \begin{pmatrix} \sin\eta\cos\upsilon \\ \sin\eta\sin\upsilon \\ \cos\eta \end{pmatrix} \mapsto \vec{b}_x^B = \begin{pmatrix} \sin(0.34\pi)\cos\upsilon \\ \sin(0.34\pi)\sin\upsilon \\ \cos(0.34\pi) \end{pmatrix}. \quad (21)
$$

Substituting Eq. (21) into Eq. (3), the vendor can obtain a new vector $\vec{n}_x^B$ instead of the original vector $\vec{n}$. Then, from Eq. (14), Alice and Bob can obtain the result of $\text{CHSH}_x^B \approx 1.9 < 2$, which will not cause the violation of inequality. Meanwhile, according to Eq. (9), in the range of Eq. (20)-(i), the average fidelity of classical simulation is

$$
\begin{aligned}
\bar{F}_1 &= \frac{1}{4} + \int \frac{2 V_{c_0 c_1}(\vec{n}) \cdot \vec{n}}{4} = \frac{1}{4} + \frac{1}{2} \int \vec{n}_x^B \cdot \vec{n} \\
&= \frac{1}{4} + \frac{1}{2} \frac{\int_0^{2\pi}\int_0^{2\pi}\int_0^{0.4\pi}\int_0^{0.32\pi} \vec{n}_x^B \cdot \vec{n}\, \sin\theta\sin\eta\, d\eta d\theta d\upsilon d\phi}{\int_0^{2\pi}\int_0^{2\pi}\int_0^{0.4\pi}\int_0^{0.32\pi} \sin\theta\sin\eta\, d\eta d\theta d\upsilon d\phi} \\
&\approx 0.8983.
\end{aligned} \quad (22)
$$

Similarly, in the range of Eq.(20)-(ii), the average fidelity of classical simulation is

$$
\begin{aligned}
\bar{F}_2 &= \frac{1}{4} + \int \frac{2 V_{c_0 c_1}(\vec{n}) \cdot \vec{n}}{4} = \frac{1}{4} + \frac{1}{2} \int \vec{n}_x^B \cdot \vec{n} \\
&= \frac{1}{4} + \frac{1}{2} \frac{\int\int\int_{0.276\pi}^{0.724\pi}\int_{0.1\pi}^{0.9\pi} \vec{n}_x^B \cdot \vec{n}\, \sin\theta\sin\eta\, d\eta\, d\theta d\upsilon d\phi}{\int\int\int_{0.276\pi}^{0.724\pi}\int_{0.1\pi}^{0.9\pi} \sin\theta\sin\eta\, d\eta\, d\theta d\upsilon d\phi} \\
&\approx 0.7924.
\end{aligned} \quad (23)
$$

For the area outside the range described in Eq. (20), the input vectors $\vec{a}$ and $\vec{b}$ will not cause CHSH > 2. According to Ho's protocol, these vectors can be teleported with perfect fidelity, and for such inputs we have $\bar{F}_3 = 1$.

The overall average fidelity of our classical simulation protocol P_{Gate} is

$$
\begin{aligned}
\bar{F}_p &= \frac{1}{16\pi^2} \cdot \{[2\pi \times (1 - 0.536) \times 2\pi \times (1 - 0.309)] \cdot \bar{F}_1 \\
&\quad + [0.638\pi \times 0.647 \times 2 \times 0.8\pi \times 0.951 \times 2] \cdot \bar{F}_2\} \\
&\quad + \frac{1}{16\pi^2} \cdot \{16\pi^2 - [2\pi \times (1 - 0.536) \times 2\pi \\
&\quad \times (1 - 0.309)] - [0.638\pi \times 0.647 \times 2 \times 0.8\pi \\
&\quad \times 0.951 \times 2]\} \bar{F}_3 \approx 0.9755.
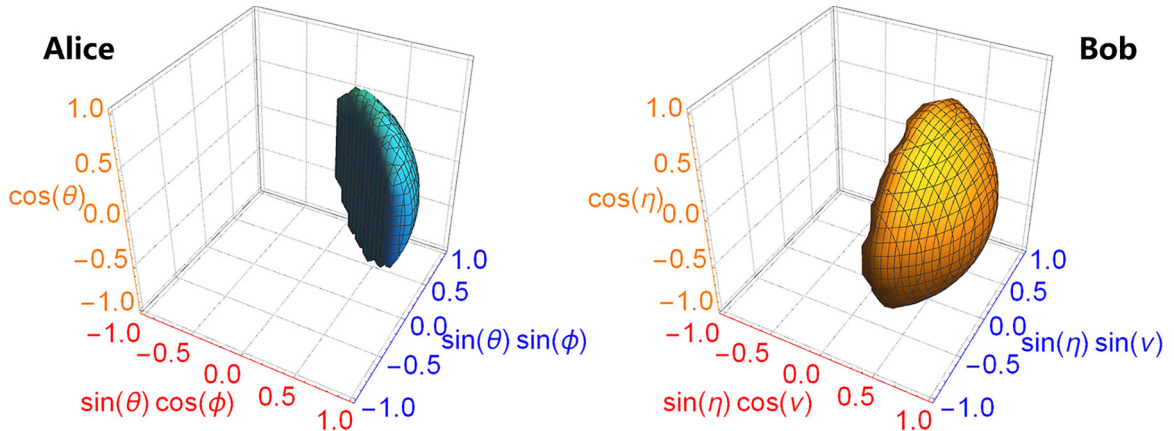\end{aligned} \quad (24)
$$

FIG. 4. The second input range of Alice and Bob that makes the inequality violated. The blue arc surface represents Alice's input range and the yellow one represents Bob's input range: $0.276\pi < \theta < 0.724\pi$ and $0 \leqslant \phi < 0.569\pi$ or $1.931\pi < \phi \leqslant 2\pi$; $0.1\pi < \eta < 0.9\pi$ and $0 \leqslant \upsilon < 0.4\pi$ or $1.6\pi < \upsilon \leqslant 2\pi$

According to the above analysis, Eq. (24) is the maximum value that can be achieved by classical simulations of CNOT-QGT systems, which actually provides another boundary for evaluating the quantumness of a CNOT-QGT black-box system. If the average fidelity of the system is greater than 97.55%, it can be considered that the possibility of high fidelity classical simulation in the black-box system is very low. This also shows that with this local simulation method, vendors can use purely classical methods to forge the QGT protocol and still output high average fidelity results. In this case, only measuring the fidelity of the QGT system will not fully guarantee the security. If the average fidelity of the system only exceeds the lower bound of the fidelity given in Eq. (17), the determination of the quantumness of the system may be positive. However, to eliminate the pseudointerference of the high-fidelity classical simulation scheme and improve the reliability of verification, it is necessary to further measure the CHSH value to confirm the quantumness of the system to fully evaluate the implementation effect of the scheme.

B. Security assessment of high-fidelity and high-inequality violations

In the Sec. IV A, one mainly consider the situation of maximizing the average fidelity of classical simulation without CHSH > 2. Further consider the situation that the vendor uses other simulation states for substitution. Taking the input state $\vec{a}_0 = (0, 0, 1)$, $\vec{b}_0 = (0, 0, 1)$, and $\vec{a}_1 = (\frac{1}{\sqrt{2}}, \frac{1}{\sqrt{2}}, 0)$, $\vec{b}_1 = (1, 0, 0)$ that can maximize the CHSH value given in Eq. (14) as the example (where $\theta_0 = 0$, $\phi_0 = 0$, $\eta_0 = 0$, $\upsilon_0 = \frac{\pi}{2}$, $\theta_1 = \frac{\pi}{2}$, $\phi_1 = \frac{\pi}{4}$, $\eta_1 = \frac{\pi}{2}$, $\upsilon_1 = 0$). In this situation, the maximum CHSH value can be obtained, which is about 2.5908, while the corresponding overall average simulation fidelity is $\bar{F}_P \approx 94.17\%$. A more general simulated states form for CHSH verification can be denoted as

$$\theta_0' = 0 + \theta_x^B, \quad \eta_0' = 0 + \eta_x^B,$$

$$\theta_1' = \frac{\pi}{2} - \frac{13}{37}\theta_x^B, \quad \eta_1' = \frac{\pi}{2} - \frac{8}{17}\eta_x^B. \quad (25)$$

Here, θ_x^B and η_x^B are the deviations between a input sates and simulation states. One choose the starting point of simulation state group as $\{\theta_0 = \eta_0 = 0, \phi_0 = 0, \upsilon_0 = \frac{\pi}{2}, \theta_1 = \eta_1 = \frac{\pi}{2}, \phi_1 = \frac{\pi}{4}, \upsilon_1 = 0\}$, i.e., $\theta_x^B = 0$, $\eta_x^B = 0$; and the endpoint of simulation state group as $\{\theta_0 = \theta_1 = 0.37\pi, \eta_0 = \eta_1 = 0.34\pi, \phi_0 = 0, \upsilon_0 = \frac{\pi}{2}, \phi_1 = 0.21\pi, \upsilon_1 = 0\}$, i.e., $\theta_x^B = 0.37\pi$, $\eta_x^B = 0.34\pi$, which is the simulated state that maximizes the fidelity as Eq. (21).

To clearly illustrate the performance of classical simulation, we numerically calculated the simulation CHSH value and the simulation average fidelity as a function of θ_x^B and η_x^B. The results are shown in Fig. 5. From Fig. 5 one can see that the simulation average fidelity increases with the increase of θ_x^B and η_x^B [as shown in Fig. 5(a)], and the simulation CHSH value decreases with the increase of θ_x^B and η_x^B [as shown in Fig. 5(b)]. It seems to be a negative correlation between the classical simulation average fidelity and the CHSH violation. To better represent this negative correlation relationship, we drew the boundary extreme value relationship curve between the classical simulation average fidelity and the CHSH value
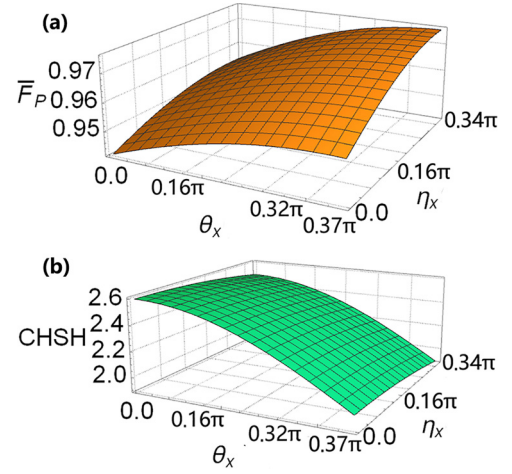
FIG. 5. Relationship between simulated state parameters θ_x^B and η_x^B and simulated average fidelity and CHSH value. Where, $\theta_x^B \in [0, 0.37\pi]$, $\eta_x^B \in [0, 0.34\pi]$. Panel (a) shows the simulated average fidelity, which increases with θ_x^B and η_x^B. Panel (b) shows the CHSH value, which decreases as θ_x^B and η_x^B increase.

under the condition of $\theta_x^B = \eta_x^B$, as shown in the red solid line in Fig. 6.

Figure 6 shows that in the case where eavesdropping exists and the eavesdropper can perform classical simulation forgery based on the eavesdropped information, the verification method relying only on the average fidelity or CHSH violation may not be completely credible. In the Fig. 6 that the red region represents where classical simulation exists. The range above the red solid line (green range) in Fig. 6 can be considered as an area that cannot be achieved under this classical simulation and the combination of (CHSH, $\bar{F}_P$) values given by the red solid line is the corresponding threshold for security assessment.
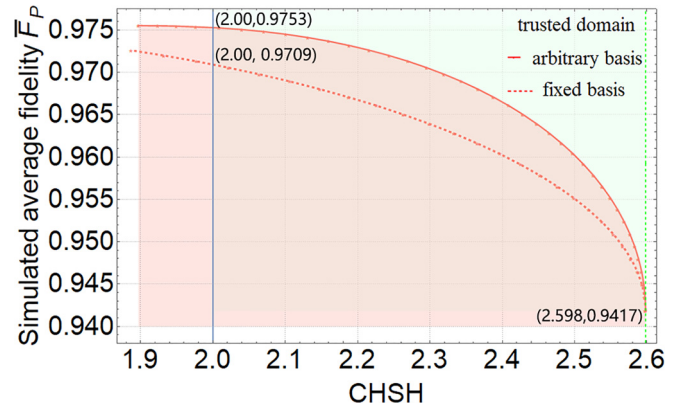
FIG. 6. The correspondence between the classical simulation average fidelity $\bar{F}_P$ and the CHSH value in the case of classical simulation. The red solid line is the relationship between the $\bar{F}_P$ and the CHSH maximum on an arbitrary measurement basis, and when CHSH = 2, the $\bar{F}_P$ is about 97.53%; The red dotted line is the correspondence between the $\bar{F}_P$ and the CHSH value when the measurement basis is fixed (fixed as the measurement basis discussed above which can maximize the CHSH value). When the verification results of the inequality and fidelity are in the green area of the figure, the CNOT-QGT system can be considered safe and reliable.

The verification method based on nonlocality can verify the security loopholes of the commonly used method of taking fidelity as the performance criterion of the QGT scheme. The best method to evaluate the implementation effect and security of CNOT-QGT system should be based on the double criteria of "high inequality violation and high fidelity." When the verification results have high inequality violation and fidelity at the same time, that is, they are located in the green area in Fig. 6, the black-box system can be considered safe and reliable. Otherwise, the QGT system is not credible.

V. CONCLUSION AND SUMMARY

In this paper, the double verification criteria of "high-fidelity and high-inequality violation" for the CNOT-QGT process are proposed, and the basic principle of the reliability verification mechanism of the quantum gate teleportation scheme is clarified. The assumption of the black-box scenario in this verification scheme protects the supplier's equipment information, and at the same time, the scheme avoids the possibility of the vendor using classical resources to simulate fraud. Therefore, our verification scheme ensures the bidirectional security of the QGT implementation process. Not only can the classic simulation schemes with high fidelity, such as the Gisin model [18] and Ho's model [16], be detected by our verification methods, but also the nonuniform bilateral Bloch ball compression method with higher fidelity can be effectively detected by our scheme.

In terms of experimental verifiability, it is mainly necessary to consider the two parts that make up the QGT nonlocality verification experiment, namely, (1) the QGT experimental implementation system and (2) independent measurements of quantum states A and B. Compared with QGT, the verification scheme based on nonlocality assessment in this work only adjusts the release time of classical information (c_0, c_1) and adds measurement for the target state system. Therefore, in principle, all experimental systems that can complete QGT with high quality can complete our plan. This paper presents an important parameter that characterizes the impact of noise in the implementation of CNOT gate teleportation. Under optimal parameter conditions, when $\mu > 0.7698$, the CHSH value is greater than 2, which violates the CHSH inequality. That is, when the implementation fidelity of the CNOT gate scheme is greater than 0.8274, the violation of the CHSH inequality can be detected. According to the existing CNOT-QGT experiments based on linear optical systems [5], trapped-ion system [6], and so on, the fidelity of these experimental systems are all greater than 0.84. Therefore, our scheme can be effectively demonstrated in these QGT experimental systems.

This study proposes a reliable verification method for QGT based on the nonlocality characteristics of entangled quantum resources to address the issue of untrusted vendors. In future research work, we also hope to further promote the application of this scheme. For example, how to apply the resource verification scheme based on Bell nonlocality in the black-box scenario of controlled quantum teleportation with a third party is an important question. On the other hand, the work of this paper uses CHSH inequality to verify Bell's nonlocality, so is it possible to find a better boundary by using inequalities other than CHSH? These questions are expected to be answered in future research.

APPENDIX A: GENERATOR OF Su(4) GROUP

The generator of Su(4) group

$$\lambda_1 = \begin{pmatrix} 0 & 1 & 0 & 0 \\ 1 & 0 & 0 & 0 \\ 0 & 0 & 0 & 0 \\ 0 & 0 & 0 & 0 \end{pmatrix}, \quad \lambda_2 = \begin{pmatrix} 0 & -i & 0 & 0 \\ i & 0 & 0 & 0 \\ 0 & 0 & 0 & 0 \\ 0 & 0 & 0 & 0 \end{pmatrix}, \quad \lambda_3 = \begin{pmatrix} 1 & 0 & 0 & 0 \\ 0 & -1 & 0 & 0 \\ 0 & 0 & 0 & 0 \\ 0 & 0 & 0 & 0 \end{pmatrix}, \quad \lambda_4 = \begin{pmatrix} 0 & 0 & 1 & 0 \\ 0 & 0 & 0 & 0 \\ 1 & 0 & 0 & 0 \\ 0 & 0 & 0 & 0 \end{pmatrix},$$

$$\lambda_5 = \begin{pmatrix} 0 & 0 & -i & 0 \\ 0 & 0 & 0 & 0 \\ i & 0 & 0 & 0 \\ 0 & 0 & 0 & 0 \end{pmatrix}, \quad \lambda_6 = \begin{pmatrix} 0 & 0 & 0 & 0 \\ 0 & 0 & 1 & 0 \\ 0 & 1 & 0 & 0 \\ 0 & 0 & 0 & 0 \end{pmatrix}, \quad \lambda_7 = \begin{pmatrix} 0 & 0 & 0 & 0 \\ 0 & 0 & -i & 0 \\ 0 & i & 0 & 0 \\ 0 & 0 & 0 & 0 \end{pmatrix}, \quad \lambda_8 = \frac{1}{\sqrt{3}} \begin{pmatrix} 1 & 0 & 0 & 0 \\ 0 & 1 & 0 & 0 \\ 0 & 0 & -2 & 0 \\ 0 & 0 & 0 & 0 \end{pmatrix},$$

$$\lambda_9 = \begin{pmatrix} 0 & 0 & 0 & 1 \\ 0 & 0 & 0 & 0 \\ 0 & 0 & 0 & 0 \\ 1 & 0 & 0 & 0 \end{pmatrix}, \quad \lambda_{10} = \begin{pmatrix} 0 & 0 & 0 & -i \\ 0 & 0 & 0 & 0 \\ 0 & 0 & 0 & 0 \\ i & 0 & 0 & 0 \end{pmatrix}, \quad \lambda_{11} = \begin{pmatrix} 0 & 0 & 0 & 0 \\ 0 & 0 & 0 & 1 \\ 0 & 0 & 0 & 0 \\ 0 & 1 & 0 & 0 \end{pmatrix}, \quad \lambda_{12} = \begin{pmatrix} 0 & 0 & 0 & 0 \\ 0 & 0 & 0 & -i \\ 0 & 0 & 0 & 0 \\ 0 & i & 0 & 0 \end{pmatrix},$$

$$\lambda_{13} = \begin{pmatrix} 0 & 0 & 0 & 0 \\ 0 & 0 & 0 & 0 \\ 0 & 0 & 0 & 1 \\ 0 & 0 & 1 & 0 \end{pmatrix}, \quad \lambda_{14} = \begin{pmatrix} 0 & 0 & 0 & 0 \\ 0 & 0 & 0 & 0 \\ 0 & 0 & 0 & -i \\ 0 & 0 & i & 0 \end{pmatrix}, \quad \lambda_{15} = \frac{1}{\sqrt{6}} \begin{pmatrix} 1 & 0 & 0 & 0 \\ 0 & 1 & 0 & 0 \\ 0 & 0 & 1 & 0 \\ 0 & 0 & 0 & -3 \end{pmatrix}.$$

APPENDIX B: FIFTEEN-DIMENSIONAL FORM OF THIS PAPER

1. Fifteen-dimensional Bloch-vector form of $|z^j\rangle$

According to the discussion in the paper, for the measurement base $\vec{z}$ composed of $\vec{z}_a = (x_a, y_a, z_a)$ and $\vec{z}_b = (x_b, y_b, z_b)$, there are four corresponding projection directions of equal probability distribution. According to Eqs. (1) and (2), the Bloch vectors corresponding to these four projection directions are, respectively,

(i) $|z^1\rangle \rightarrow \vec{z^1} = \vec{z} = [\frac{x_b}{2}(1+z_a), \frac{y_b}{2}(1+z_a), \frac{z_b}{2}(1+z_a), \frac{x_a}{2}(1+z_b), \frac{y_a}{2}(1+z_b), \frac{1}{2}(x_ax_b + y_ay_b), \frac{1}{2}(y_ax_b - x_ay_b), \frac{1}{2\sqrt{3}}(z_az_b + 2z_a - z_b), \frac{1}{2}(x_ax_b - y_ay_b), \frac{1}{2}(y_ax_b + x_ay_b), \frac{x_a}{2}(1-z_b), \frac{y_a}{2}(1-z_b), \frac{x_b}{2}(1-z_a), \frac{y_b}{2}(1-z_a), \frac{1}{\sqrt{6}}(z_a + z_b - z_az_b)];$

(ii) $|z^2\rangle \rightarrow \vec{z^2} = [-\frac{x_b}{2}(1-z_a), -\frac{y_b}{2}(1-z_a), -\frac{z_b}{2}(1-z_a), -\frac{x_a}{2}(1-z_b), -\frac{y_a}{2}(1-z_b), \frac{1}{2}(x_ax_b + y_ay_b), \frac{1}{2}(y_ax_b - x_ay_b), \frac{1}{2\sqrt{3}}(z_az_b - 2z_a + z_b), \frac{1}{2}(x_ax_b - y_ay_b), \frac{1}{2}(y_ax_b + x_ay_b), -\frac{x_a}{2}(1+z_b), -\frac{y_a}{2}(1+z_b), -\frac{x_b}{2}(1+z_a), -\frac{y_b}{2}(1+z_a), \frac{1}{\sqrt{6}}(-z_a - z_b - z_az_b)];$

(iii) $|z^3\rangle \rightarrow \vec{z^3} = [\frac{x_b}{2}(1-z_a), \frac{y_b}{2}(1-z_a), \frac{z_b}{2}(1-z_a), -\frac{x_a}{2}(1+z_b), -\frac{y_a}{2}(1+z_b), -\frac{1}{2}(x_ax_b + y_ay_b), -\frac{1}{2}(y_ax_b - x_ay_b), \frac{1}{2\sqrt{3}}(-z_az_b - 2z_a - z_b), -\frac{1}{2}(x_ax_b - y_ay_b), -\frac{1}{2}(y_ax_b + x_ay_b), -\frac{x_a}{2}(1-z_b), -\frac{y_a}{2}(1-z_b), \frac{x_b}{2}(1+z_a), \frac{y_b}{2}(1+z_a), \frac{1}{\sqrt{6}}(-z_a + z_b + z_az_b)];$

(iv) $|z^4\rangle \rightarrow \vec{z^4} = [-\frac{x_b}{2}(1+z_a), -\frac{y_b}{2}(1+z_a), -\frac{z_b}{2}(1+z_a), \frac{x_a}{2}(1-z_b), \frac{y_a}{2}(1-z_b), -\frac{1}{2}(x_ax_b + y_ay_b), -\frac{1}{2}(y_ax_b - x_ay_b), \frac{1}{2\sqrt{3}}(-z_az_b + 2z_a + z_b), -\frac{1}{2}(x_ax_b - y_ay_b), -\frac{1}{2}(y_ax_b + x_ay_b), \frac{x_a}{2}(1+z_b), \frac{y_a}{2}(1+z_b), -\frac{x_b}{2}(1-z_a), -\frac{y_b}{2}(1-z_a), \frac{1}{\sqrt{6}}(z_a - z_b + z_az_b)].$

2. Fifteen-dimensional unitary matrix form of R_{c_0,c_1}

In the ideal teleportation simulation of the system in this paper, with (c_0, c_1) as the condition, the teleportation state contained in boxes for

$$\rho_{A,B} = \frac{1}{4}\mathbb{I}_4 + \frac{1}{2}[(R_{c_0,c_1} \cdot \vec{n}) \cdot \vec{\lambda}], \tag{B1}$$

where $\vec{n}' = R_{c_0,c_1} \cdot \vec{n}$, and $R_{00} = \mathbb{I}, R_{01} = R_a(\hat{z}, \pi), R_{10} = R_b(\hat{x}, \pi)$, and $R_{11} = R_a(\hat{z}, \pi)$, and $R_b(\hat{x}, \pi)$. R_{c_0,c_1} represents the local operation on the input states of Alice and Bob, and $R_j(\hat{i}, \pi)$ represents the rotation π of the vector $\vec{j}$ corresponding to the input state along the orthogonal direction corresponding to the σ_i operator, that is,

(i) $R_{00} = \mathbb{I} : \vec{a} = (a_1, a_2, a_3), \vec{b} = (b_1, b_2, b_3) \rightarrow \vec{a}' = (a_1, a_2, a_3), \vec{b}' = (b_1, b_2, b_3);$
(ii) $R_{01} = R_a(\hat{z}, \pi) : \vec{a} = (a_1, a_2, a_3), \vec{b} = (b_1, b_2, b_3) \rightarrow \vec{a}' = (-a_1, -a_2, a_3), \vec{b}' = (b_1, b_2, b_3);$
(iii) $R_{10} = R_b(\hat{x}, \pi) : \vec{a} = (a_1, a_2, a_3), \vec{b} = (b_1, b_2, b_3) \rightarrow \vec{a}' = (a_1, a_2, a_3), \vec{b}' = (b_1, -b_2, -b_3);$
(iv) $R_{11} = R_a(\hat{z}, \pi) \& R_b(\hat{x}, \pi) : \vec{a} = (a_1, a_2, a_3), \vec{b} = (b_1, b_2, b_3) \rightarrow \vec{a}' = (-a_1, -a_2, a_3), \vec{b}' = (b_1, -b_2, -b_3).$

Then, the method of constructing 15-dimensional Bloch vectors corresponding to four-dimensional separable states and four-dimensional CNOT gate states based on two-dimensional states, that is, Eqs. (2) and (3), can obtain the 15-dimensional

unitary matrix form of R_{c_0,c_1}:

$$R_{00} = \mathbb{I}_{15};$$

$$R_{01} = \begin{pmatrix}
1 & 0 & 0 & 0 & 0 & 0 & 0 & 0 & 0 & 0 & 0 & 0 & 0 & 0 & 0 \\
0 & 1 & 0 & 0 & 0 & 0 & 0 & 0 & 0 & 0 & 0 & 0 & 0 & 0 & 0 \\
0 & 0 & 1 & 0 & 0 & 0 & 0 & 0 & 0 & 0 & 0 & 0 & 0 & 0 & 0 \\
0 & 0 & 0 & -1 & 0 & 0 & 0 & 0 & 0 & 0 & 0 & 0 & 0 & 0 & 0 \\
0 & 0 & 0 & 0 & -1 & 0 & 0 & 0 & 0 & 0 & 0 & 0 & 0 & 0 & 0 \\
0 & 0 & 0 & 0 & 0 & -1 & 0 & 0 & 0 & 0 & 0 & 0 & 0 & 0 & 0 \\
0 & 0 & 0 & 0 & 0 & 0 & -1 & 0 & 0 & 0 & 0 & 0 & 0 & 0 & 0 \\
0 & 0 & 0 & 0 & 0 & 0 & 0 & 1 & 0 & 0 & 0 & 0 & 0 & 0 & 0 \\
0 & 0 & 0 & 0 & 0 & 0 & 0 & 0 & -1 & 0 & 0 & 0 & 0 & 0 & 0 \\
0 & 0 & 0 & 0 & 0 & 0 & 0 & 0 & 0 & -1 & 0 & 0 & 0 & 0 & 0 \\
0 & 0 & 0 & 0 & 0 & 0 & 0 & 0 & 0 & 0 & -1 & 0 & 0 & 0 & 0 \\
0 & 0 & 0 & 0 & 0 & 0 & 0 & 0 & 0 & 0 & 0 & -1 & 0 & 0 & 0 \\
0 & 0 & 0 & 0 & 0 & 0 & 0 & 0 & 0 & 0 & 0 & 0 & 1 & 0 & 0 \\
0 & 0 & 0 & 0 & 0 & 0 & 0 & 0 & 0 & 0 & 0 & 0 & 0 & 1 & 0 \\
0 & 0 & 0 & 0 & 0 & 0 & 0 & 0 & 0 & 0 & 0 & 0 & 0 & 0 & 1
\end{pmatrix}, \tag{B2}$$

$$R_{10} = \begin{pmatrix}
1 & 0 & 0 & 0 & 0 & 0 & 0 & 0 & 0 & 0 & 0 & 0 & 0 & 0 & 0 \\
0 & -1 & 0 & 0 & 0 & 0 & 0 & 0 & 0 & 0 & 0 & 0 & 0 & 0 & 0 \\
0 & 0 & -1 & 0 & 0 & 0 & 0 & 0 & 0 & 0 & 0 & 0 & 0 & 0 & 0 \\
0 & 0 & 0 & 0 & 0 & 0 & 0 & 0 & 0 & 0 & 1 & 0 & 0 & 0 & 0 \\
0 & 0 & 0 & 0 & 0 & 0 & 0 & 0 & 0 & 0 & 0 & 1 & 0 & 0 & 0 \\
0 & 0 & 0 & 0 & 0 & 0 & 0 & 0 & 1 & 0 & 0 & 0 & 0 & 0 & 0 \\
0 & 0 & 0 & 0 & 0 & 0 & 0 & 0 & 0 & 1 & 0 & 0 & 0 & 0 & 0 \\
0 & 0 & 0 & 0 & 0 & 0 & 0 & \frac{1}{3} & 0 & 0 & 0 & 0 & 0 & 0 & \frac{2\sqrt{2}}{3} \\
0 & 0 & 0 & 0 & 0 & 1 & 0 & 0 & 0 & 0 & 0 & 0 & 0 & 0 & 0 \\
0 & 0 & 0 & 0 & 0 & 0 & 1 & 0 & 0 & 0 & 0 & 0 & 0 & 0 & 0 \\
0 & 0 & 0 & 1 & 0 & 0 & 0 & 0 & 0 & 0 & 0 & 0 & 0 & 0 & 0 \\
0 & 0 & 0 & 0 & 1 & 0 & 0 & 0 & 0 & 0 & 0 & 0 & 0 & 0 & 0 \\
0 & 0 & 0 & 0 & 0 & 0 & 0 & 0 & 0 & 0 & 0 & 0 & 1 & 0 & 0 \\
0 & 0 & 0 & 0 & 0 & 0 & 0 & 0 & 0 & 0 & 0 & 0 & 0 & -1 & 0 \\
0 & 0 & 0 & 0 & 0 & 0 & 0 & \frac{2\sqrt{2}}{3} & 0 & 0 & 0 & 0 & 0 & 0 & -\frac{1}{3}
\end{pmatrix},$$

$$R_{11} = \begin{pmatrix}
1 & 0 & 0 & 0 & 0 & 0 & 0 & 0 & 0 & 0 & 0 & 0 & 0 & 0 & 0 \\
0 & -1 & 0 & 0 & 0 & 0 & 0 & 0 & 0 & 0 & 0 & 0 & 0 & 0 & 0 \\
0 & 0 & -1 & 0 & 0 & 0 & 0 & 0 & 0 & 0 & 0 & 0 & 0 & 0 & 0 \\
0 & 0 & 0 & 0 & 0 & 0 & 0 & 0 & 0 & 0 & -1 & 0 & 0 & 0 & 0 \\
0 & 0 & 0 & 0 & 0 & 0 & 0 & 0 & 0 & 0 & 0 & -1 & 0 & 0 & 0 \\
0 & 0 & 0 & 0 & 0 & 0 & 0 & 0 & -1 & 0 & 0 & 0 & 0 & 0 & 0 \\
0 & 0 & 0 & 0 & 0 & 0 & 0 & 0 & 0 & -1 & 0 & 0 & 0 & 0 & 0 \\
0 & 0 & 0 & 0 & 0 & 0 & 0 & \frac{1}{3} & 0 & 0 & 0 & 0 & 0 & 0 & \frac{2\sqrt{2}}{3} \\
0 & 0 & 0 & 0 & 0 & -1 & 0 & 0 & 0 & 0 & 0 & 0 & 0 & 0 & 0 \\
0 & 0 & 0 & 0 & 0 & 0 & -1 & 0 & 0 & 0 & 0 & 0 & 0 & 0 & 0 \\
0 & 0 & 0 & -1 & 0 & 0 & 0 & 0 & 0 & 0 & 0 & 0 & 0 & 0 & 0 \\
0 & 0 & 0 & 0 & -1 & 0 & 0 & 0 & 0 & 0 & 0 & 0 & 0 & 0 & 0 \\
0 & 0 & 0 & 0 & 0 & 0 & 0 & 0 & 0 & 0 & 0 & 0 & 1 & 0 & 0 \\
0 & 0 & 0 & 0 & 0 & 0 & 0 & 0 & 0 & 0 & 0 & 0 & 0 & -1 & 0 \\
0 & 0 & 0 & 0 & 0 & 0 & 0 & \frac{2\sqrt{2}}{3} & 0 & 0 & 0 & 0 & 0 & 0 & -\frac{1}{3}
\end{pmatrix}. \tag{B3}$$

[1] C. H. Bennett, G. Brassard, C. Crépeau, R. Jozsa, A. Peres, and W. K. Wootters, Teleporting an Unknown Quantum State Via Dual Classical and Einstein-Podolsky-Rosen Channels, Phys. Rev. Lett. **70**, 1895 (1993).

[2] D. Gottesman and I. L. Chuang, Demonstrating the viability of universal quantum computation using teleportation and single-qubit operations, Nature (London) **402**, 390 (1999).

[3] J. I. Cirac, A. K. Ekert, S. F. Huelga, and C. Macchiavello, Distributed quantum computation over noisy channels, Phys. Rev. A **59**, 4249 (1999).

[4] D. P. DiVincenzo, The physical implementation of quantum computation, Fortschr. Phys. **48**, 771 (2000).

[5] Y.-F. Huang, X.-F. Ren, Y.-S. Zhang, L.-M. Duan, and G.-C. Guo, Experimental Teleportation of a Quantum Controlled-NOT Gate, Phys. Rev. Lett. **93**, 240501 (2004).

[6] Y. Wan, D. Kienzler, S. D. Erickson, K. H. Mayer, T. R. Tan, J. J. Wu, H. M. Vasconcelos, S. Glancy, E. Knill, D. J. Wineland *et al.*, Quantum gate teleportation between separated qubits in a trapped-ion processor, Science **364**, 875 (2019).

[7] J. Eisert, K. Jacobs, P. Papadopoulos, and M. B. Plenio, Optimal local implementation of nonlocal quantum gates, Phys. Rev. A **62**, 052317 (2000).

[8] D. Wang, Y. Liu, J. Ding, X. Qiang, Y. Liu, A. Huang, X. Fu, P. Xu, M. Deng, X. Yang, and J. Wu, Remote-controlled quantum computing by quantum entanglement, Opt. Lett. **45**, 6298 (2020).

[9] X.-Q. Zhou, T. C. Ralph, P. Kalasuwan, M. Zhang, A. Peruzzo, B. P. Lanyon, and J. L. O'brien, Adding control to arbitrary unknown quantum operations, Nat. Commun. **2**, 413 (2011).

[10] S. D. Bartlett and W. J. Munro, Quantum Teleportation of Optical Quantum Gates, Phys. Rev. Lett. **90**, 117901 (2003).

[11] C. A. Pérez-Delgado and J. F. Fitzsimons, Iterated Gate Teleportation and Blind Quantum Computation, Phys. Rev. Lett. **114**, 220502 (2015).

[12] H.-F. Wang, A.-D. Zhu, S. Zhang, and K.-H. Yeon, Optically controlled phase gate and teleportation of a controlled-not gate for spin qubits in a quantum-dot–microcavity coupled system, Phys. Rev. A **87**, 062337 (2013).

[13] S. Hu, W.-X. Cui, D.-Y. Wang, C.-H. Bai, Q. Guo, H.-F. Wang, A.-D. Zhu, and S. Zhang, Teleportation of a toffoli gate among distant solid-state qubits with quantum dots embedded in optical microcavities, Sci. Rep. **5**, 11321 (2015).

[14] K. S. Chou, J. Z. Blumoff, C. S. Wang, P. C. Reinhold, C. J. Axline, Y. Y. Gao, L. Frunzio, M. Devoret, L. Jiang, and R. Schoelkopf, Deterministic teleportation of a quantum gate between two logical qubits, Nature (London) **561**, 368 (2018).

[15] R. Clifton and D. Pope, On the nonlocality of the quantum channel in the standard teleportation protocol, Phys. Lett. A **292**, 1 (2001).

[16] M. Ho, J.-D. Bancal, and V. Scarani, Device-independent certification of the teleportation of a qubit, Phys. Rev. A **88**, 052318 (2013).

[17] S. Popescu, Bell's Inequalities Versus Teleportation: What is Nonlocality? Phys. Rev. Lett. **72**, 797 (1994).

[18] N. Gisin, Nonlocality criteria for quantum teleportation, Phys. Lett. A **210**, 157 (1996).

[19] A. Acín, S. Massar, and S. Pironio, Efficient quantum key distribution secure against no-signalling eavesdroppers, New J. Phys. **8**, 126 (2006).

[20] A. Acín, N. Brunner, N. Gisin, S. Massar, S. Pironio, and V. Scarani, Device-Independent Security of Quantum Cryptography against Collective Attacks, Phys. Rev. Lett. **98**, 230501 (2007).

[21] S. Pironio, A. Acín, N. Brunner, N. Gisin, S. Massar, and V. Scarani, Device-independent quantum key distribution secure against collective attacks, New J. Phys. **11**, 045021 (2009).

[22] N. Brunner, D. Cavalcanti, S. Pironio, V. Scarani, and S. Wehner, Bell nonlocality, Rev. Mod. Phys. **86**, 419 (2014).

[23] J. S. Bell, On the einstein podolsky rosen paradox, Phys. Phys. Fiz. **1**, 195 (1964).

[24] X.-S. Ma, T. Herbst, T. Scheidl, D. Wang, S. Kropatschek, W. Naylor, B. Wittmann, A. Mech, J. Kofler, E. Anisimova *et al.*, Quantum teleportation over 143 kilometres using active feed-forward, Nature (London) **489**, 269 (2012).

[25] L. Jakóbczyk and M. Siennicki, Geometry of bloch vectors in two-qubit system, Phys. Lett. A **286**, 383 (2001).

[26] J. F. Clauser, M. A. Horne, A. Shimony, and R. A. Holt, Proposed Experiment to Test Local Hidden-Variable Theories, Phys. Rev. Lett. **23**, 880 (1969).

[27] A. Barenco, C. H. Bennett, R. Cleve, D. P. DiVincenzo, N. Margolus, P. Shor, T. Sleator, J. A. Smolin, and H. Weinfurter, Elementary gates for quantum computation, Phys. Rev. A **52**, 3457 (1995).

[28] G. Kimura, The bloch vector for n-level systems, Phys. Lett. A **314**, 339 (2003).

[29] B. F. Toner and D. Bacon, Communication Cost of Simulating Bell Correlations, Phys. Rev. Lett. **91**, 187904 (2003).

[30] F. Bloch, W. W. Hansen, and M. Packard, Nuclear induction, Phys. Rev. **69**, 127 (1946).

[31] M. A. Nielsen, I. Chuang, and L. K. Grover, Quantum computation and quantum information, Am. J Phys. **70**, 558 (2002).

[32] F. T. Hioe and J. H. Eberly, *n*-Level Coherence Vector and Higher Conservation Laws in Quantum Optics and Quantum Mechanics, Phys. Rev. Lett. **47**, 838 (1981).

[33] J. Pöttinger and K. Lendi, Generalized bloch equations for decaying systems, Phys. Rev. A **31**, 1299 (1985).

[34] K. Lendi, F. Farhadmotamed, and A. Van Wonderen, Regularization of quantum relative entropy in finite dimensions and application to entropy production, J. Stat. Phys. **92**, 1115 (1998).

[35] R. Alicki and K. Lendi, *Quantum Dynamical Semigroups and Applications*, Vol. 717 (Springer, New York, 1987).

[36] G. Mahler and V. A. Weberruß, Quantum dynamics, in *Quantum Networks: Dynamics of Open Nanostructures* (Springer, Berlin, 1995), pp. 171–305.

[37] R. A. Bertlmann and P. Krammer, Bloch vectors for qudits, J. Phys. A: Math. Theor. **41**, 235303 (2008).

[38] M. Raginsky, A fidelity measure for quantum channels, Phys. Lett. A **290**, 11 (2001).